DOI: 10.1111/cgf.13236

COMPUTER GRAPHICS *forum*
Volume 37 (2018), number 1 pp. 112–124

Peridynamics-Based Fracture Animation for Elastoplastic Solids

Wei Chen[1], Fei Zhu[1], Jing Zhao[2,3], Sheng Li[1] and Guoping Wang[1]

[1]Department of Computer Science, Peking University, Beijing, China
{suitmyself, feizhu, lisheng, wgp}@pku.edu.cn
[2]School of Information Science and Engineering, Yanshan University, Hebei Province, China
zhaojing@ysu.edu.cn
[3]Key Laboratory of Computer Virtual Technology and System Integration, Hebei Province, China

Abstract

In this paper, we exploit the use of peridynamics theory for graphical animation of material deformation and fracture. We present a new meshless framework for elastoplastic constitutive modelling that contrasts with previous approaches in graphics. Our peridynamics-based elastoplasticity model represents deformation behaviours of materials with high realism. We validate the model by varying the material properties and performing comparisons with finite element method (FEM) simulations. The integral-based nature of peridynamics makes it trivial to model material discontinuities, which outweighs differential-based methods in both accuracy and ease of implementation. We propose a simple strategy to model fracture in the setting of peridynamics discretization. We demonstrate that the fracture criterion combined with our elastoplasticity model could realistically produce ductile fracture as well as brittle fracture. Our work is the first application of peridynamics in graphics that could create a wide range of material phenomena including elasticity, plasticity, and fracture. The complete framework provides an attractive alternative to existing methods for producing modern visual effects.

Keywords: peridynamics, fracture, elastoplasticity

ACM CCS: I.3.7 [Computer Graphics]: Three-Dimensional Graphics and Realism—Animation

1. Introduction

The simulation of deformable materials has been an important research topic in computer graphics for decades, since the early work by Terzopoulos and colleagues [TPBF87]. One of the strongest driving forces behind the active research is the persistently growing need for higher realism from the visual effects industry. Materials in the real world exhibit complex behaviours, such as coupled elastoplastic deformations, fracture, etc. The complicated material behaviours are difficult to replicate by any single method despite the numerous ones that have been developed thus far. Existing approaches generally excel at some phenomena but would stumble (if not fail) at others. For instance, mesh-based methods [MG04, ITF04, TSIF05, SB12] are a good choice to simulate elastic deformations whereas not preferred for phenomena that involve topological changes. Particle-based methods [MCG03, PKA*05, SSC*13] are considered suitable for modelling topological changes, however the inherent loss of connectivity information would cause undesirable numerical fracture [LZLW11, ZZL*16] while simulating large deformations.

We build on recent developments of peridynamics theory in the computational physics community [Sil00, SEW*07, Mit11, ELP13, MO14] and propose a novel framework for graphical animation of varied deformation behaviours and fracture. Our aim is to enrich available options of simulation techniques for easier and better animation production. Peridynamics was first adopted to animation applications by Levine *et al.* [LBC*14] where they described a simple spring-mass system to handle brittle fracture of solids. In contrast, we handle elastoplasticity, brittle fracture and ductile fracture in a single framework. To this end, we propose several novel contributions in this work. We first present an elastoplastic constitutive model in the peridynamics-based framework with simple extension to anisotropy, and the model is validated against results produced by finite element method (FEM). Furthermore, we show that both brittle and ductile fracture phenomena can be naturally represented with nearly no effort by integrating a simple fracture criterion into this material model. This is due to the integral-based formulation of peridynamics, in which forces at a material point are computed by gathering contributions from all material points in its interaction range through integration. On the other hand, methods based on classical continuum mechanics formulate force computations with partial differential equations that fail to be applicable directly on singularities such as a crack. This feature makes our peridynamics-based framework more attractive over existing approaches for producing animations that involve fracture. Lastly, our method is simple to implement and trivially parallelizable, providing a useful alternative to previous methods for animation production.

2. Related Work

A large body of literature has been devoted to physical simulation of natural phenomena as a result of active research. A complete literature review is beyond the scope of this paper. In the following, we comment only on the representative works most related to ours.

Elastoplasticity Animation. The modelling of deformable plasticity in graphics dates back to the pioneering work by Terzopoulos and Fleischer [TF88]. O'Brien and colleagues [OBH02] incorporated a similar additive plasticity model into a finite element simulation to animate ductile fracture. The strain measure was decomposed into two components, where one is due to elastic deformation and the other due to plastic deformation. Müller *et al.* [MKN*04] applied this model in their point-based framework and simulated plastic behaviours of objects. Irving *et al.* [ITF04] presented a multiplicative formulation of plasticity and pointed out that their model was better handling finite plastic deformation than the additive one. In contrast to the additive model, they decomposed the deformation gradient into two components through multiplication. The multiplicative model was extensively used by later works to animate phenomena that involve plasticity. Bargteil *et al.* simulated large viscoplastic flow [BWHT07], Gerszewski and his colleagues animated elastoplastic solids [GBB09] and Stomakhin *et al.* modelled plasticity of snow [SSC*13], just to name a few. Unfortunately, neither of the above plasticity models applies in the peridynamics framework because there is no concept of strain nor deformation gradient in the integral-based formulation. As a result, we present a new constitutive model for peridynamics in this work to animate elastoplastic solids.

Fracture Animation. Numerous methods have been proposed on fracture animation [MBP14, WWD15] because the stunning phenomenon of fracture and failure is an indispensable visual element in animated movies and video games. Early approaches use simple schemes to model fracture, such as the finite difference method [TF88], the mass-spring system [NTB*91] and the mass-point constraint system [SWB01]. O'Brien and Hodgins [OH99] adopted techniques from continuum mechanics and presented a FEM-based method to simulate brittle fracture of solids. They later extended their method to ductile fracture by incorporating a plasticity model [OBH02]. Müller *et al.* [MMDJ01] employed a quasi-static finite element analysis to animate brittle fracture of stiff materials undergoing collisions. Parker and O'Brien [PO09] presented some useful techniques for real-time simulation of fracture in game environment. One major issue in FEM-based methods is the generation of fracture patterns on meshes, which could alter the underlying mesh topology. Early methods typically made use of simple separation along mesh element boundaries [NTB*91, MMA99, SWB01, MMDJ01] or even element deletion [FDA02]. Mesh subdivision prior to splitting could somewhat increase the available geometric details [MK00, BG00], whereas this tended to introduce elements with poor aspect ratios. Allowing failure along more arbitrary paths could generate more geometrically rich fracture patterns [NF99, OH99, OBH02], albeit at the expense of complicated re-meshing. Molino *et al.* [MBF04] proposed a virtual node algorithm to avoid the complexity of remeshing, where elements were duplicated into partially filled counterparts with virtual nodes. The virtual node algorithm was frequently used by subsequent works on fracture animation [BHTF07] and mesh cutting [SDF07, WJST14] due to its simplicity compared to re-meshing methods. Kaufmann *et al.* [KMB*09] adapted the extended finite element method (XFEM) that enriches approximation by custom-designed basis functions, instead of actual/virtual element cutting. Other representative mesh-based methods resorted to modal analysis [GMD13] and pure geometric mesh decompositions [MCK13, SO14] for real-time brittle fracture. Most recently, several works explored the boundary element method for rigid body fracture [ZBG15, HW15] where only surface meshes were employed for both representation and computation.

In contrast to mesh-based approaches, meshless methods are generally considered as a better solution for animating topological changes. Based on the moving least square (MLS) meshless framework by Müller *et al.* [MKN*04], Pauly and colleagues [PKA*05] developed a novel meshless method for fracture animation of elastoplastic solids. Their method generates detailed crack surfaces and allows arbitrary crack initiation/propagation. Steinemann *et al.* [SOG09] employed surface mesh representation in meshless framework and presented a novel surface tracking technique to efficiently split the meshless deforming objects. Inspired by the rigid body assumption for simulating brittle fracture, Liu *et al.* [LHLW11] employed quasi-static analysis in a meshless local Petrov–Galerkin framework. Stomakhin *et al.* modelled the fracture of snow using a meshless material point method [SSC*13]. Hegemann *et al.* [HJST13] combined a level set–based mesh embedding technique with the material point method to animate dynamic ductile fracture.

Peridynamics. The peridynamics theory was first proposed by Silling [Sil00] as a nonlocal reformulation of classical solid mechanics. It contrasts with classical (local) theory in that the state of a material point is influenced by not necessarily the material points located in its immediate vicinity, but also those over long distances. The governing equations of the peridynamics theory are spatial integral equations instead of partial differential equations. The theory was further developed by subsequent works [SEW*07, ELP13], and its applications to the engineering field such as multiscale material modelling [ABL*08, SC14] and fracture modelling [AXS06, SWAB10, SA14] were studied. A comprehensive review of the research literature in the computational physics community is beyond our scope, we refer the readers to the book by Madenci and Oterkus [MO14]. Levine *et al.* [LBC*14] first introduced peridynamics to graphics for fracture animation. Their method was limited to brittle fracture of isotropic elastic materials with a single Poisson ratio of 0.25. Our work, on the other hand, is a complete framework that models elastoplasticity and anisotropy under various parameter settings, representing brittle and ductile fracture with high realism.

3. Background

In the peridynamics theory, any material point $\mathbf{x}$ interacts with other material points within a distance δ. The distance δ is called the

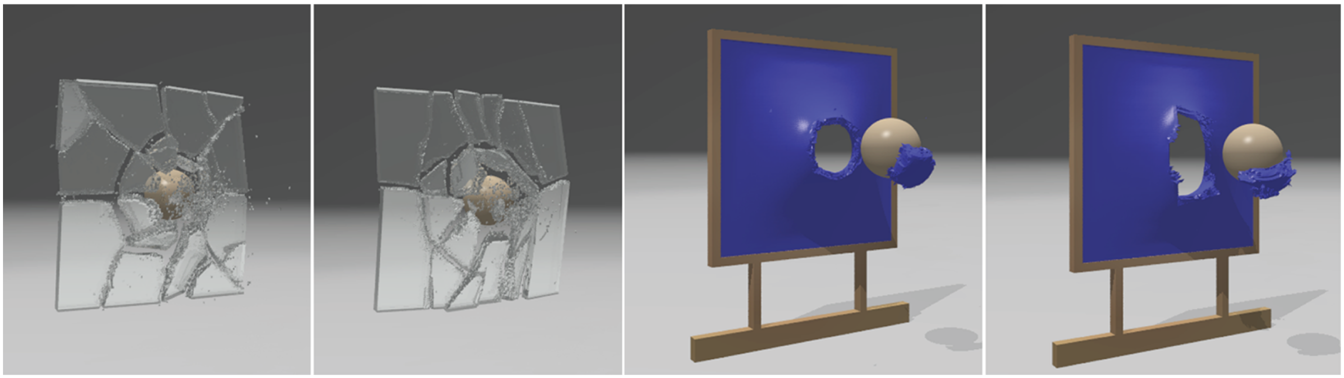

Figure 1: *A sphere shoots through walls made of different materials, causing varied fracture behaviours. From left to right: isotropic brittle fracture, anisotropic brittle fracture, isotropic ductile fracture and anisotropic ductile fracture.*

horizon of $\mathbf{x}$, and the material points within the horizon are referred as its **family**, $H_{\mathbf{x}}$. There are infinite number of family members for a material point before discretizing the continuum into discrete particles. Figure 2 is an illustration of the peridynamics discretization with particles. It seems analogous to other meshless methods based on classical theory [MCG03, MKN*04], and the difference lies in the scale of interaction radius δ. In the case of the classical (local) continuum model, the state of a particle is influenced by only particles in its immediate vicinity. For case of the peridynamics theory, however, the state of a particle is influenced by particles within a region of finite radius. The peridynamics theory is thus referred as a non-local theory. As the radius becomes infinitely large, the peridynamics theory becomes the continuous version of the molecular dynamics model. As the radius becomes smaller, it becomes the continuum mechanics model. Therefore, the peridynamics model establishes a connection between the continuum mechanics and molecular dynamics models.

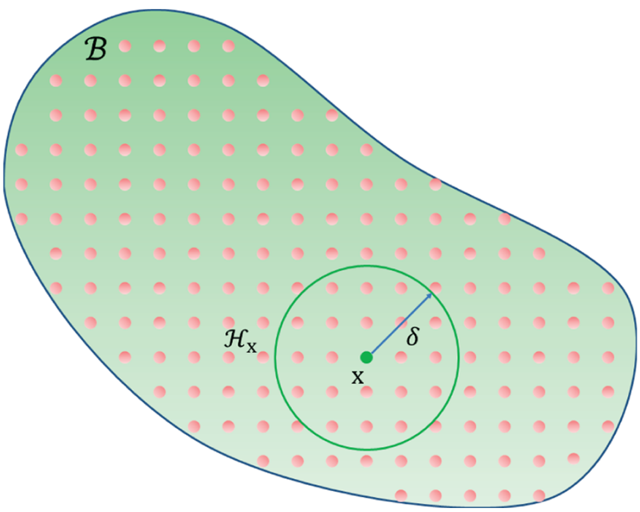

Figure 2: *Illustration of peridynamics discretization. A continuum is represented as particles (pink dots), and any particle (green dot) interacts with the particles within its horizon (green circle).*

Our motivation for choosing peridynamics is that it is more favourable to handle material discontinuities, such as cracks. This benefit inherently from an integral force formulation of its governing equations, which stands in contrast to the partial differential equations used in the classical formulations. As we know, spatial derivatives are not well defined at discontinuities. Therefore, special treatment is generally required for fracture modelling in existing methods that are based on classical continuum mechanics. For instance, the mesh-based methods [OH99, OBH02] employed remeshing operations and the meshless method by Pauly *et al.* [PKA*05] altered the particle weight functions. The peridynamics governing equations remain valid at discontinuities, and material damage is represented as part of the peridynamics constitutive model. These attributes permit fracture initiation and propagation to be modelled with arbitrary paths in the peridynamics framework.

In peridynamics, the governing equation at any point $\mathbf{x}$ is formulated in integral form as below:

$$\rho\ddot{\mathbf{u}}(\mathbf{x}) = \int_{H_{\mathbf{x}}} [\mathbf{T}\langle\mathbf{x}', \mathbf{x}\rangle - \mathbf{T}\langle\mathbf{x}, \mathbf{x}'\rangle]\mathrm{d}H + \mathbf{b}(\mathbf{x}), \tag{1}$$

where ρ is the mass density, $\mathbf{u}$ denotes the displacement, $\mathbf{b}$ is the external loads due to gravity and impact forces and $\mathbf{x}'$ is one material point that belongs to the family $H_{\mathbf{x}}$ of $\mathbf{x}$. $\mathbf{T}\langle\mathbf{x}', \mathbf{x}\rangle$ and $\mathbf{T}\langle\mathbf{x}, \mathbf{x}'\rangle$ are two essential terms in which the constitutive laws of materials are encoded. $\mathbf{T}\langle\mathbf{x}', \mathbf{x}\rangle$ represents the internal force density exerted by $\mathbf{x}'$ on $\mathbf{x}$, and $\mathbf{T}\langle\mathbf{x}, \mathbf{x}'\rangle$ is the other way around. The two terms both appear in the governing equation to enforce the Newton's third law, and

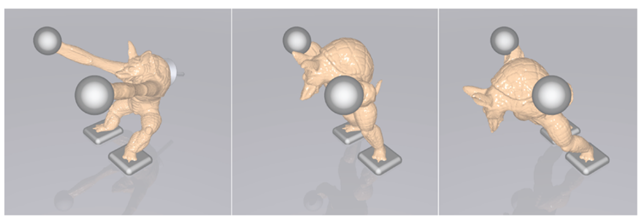

Figure 3: *An armadillo is initially anchored on its back and four limbs, and it deforms elastically when its back is released.*

similar strategy was employed in smoothed particle hydrodynamics (SPH) methods [MCG03]. The angle brackets representation $\langle\cdot\rangle$ was defined by Silling *et al.* [SEW*07] as a function inside the family $H_{\mathbf{x}}$, which they called as a **state**. Please note the integral form of the equation, which is the key difference between peridynamics and classical theory. The entire framework is built on displacements $\mathbf{u}$ instead of their spatial derivatives, thereby making discontinuity modelling trivial. With particle discretization, the integration within $H_{\mathbf{x}}$ is represented as summation over family particles:

$$\rho\ddot{\mathbf{u}}(\mathbf{x}) = \sum_{\mathbf{x}'\in H_{\mathbf{x}}} [\mathbf{T}\langle\mathbf{x}', \mathbf{x}\rangle - \mathbf{T}\langle\mathbf{x}, \mathbf{x}'\rangle] V_{\mathbf{x}'} + \mathbf{b}(\mathbf{x}), \tag{2}$$

with $V_{\mathbf{x}'}$ as the volume of particle $\mathbf{x}'$.

4. Elastoplastic Model

In this section, we describe our constitutive model for peridynamics in detail. We start with the basic isotropic elastic model, then plasticity is incorporated, and finally we extend the model with anisotropy.

4.1. Isotropic elasticity

As is discussed in Section 3, the key to peridynamics-based constitutive modelling is the design of proper internal force density $\mathbf{T}\langle\cdot\rangle$. Silling *et al.* [SEW*07] showed that peridynamic constitutive models can be designed to match many hyperelastic constitutive models under the classical elasticity theory. We derive our model based on the model described by Madenci and Oterkus [MO14], which matches the isotropic linear elasticity model in classical theory. The elastic internal force density exerted by particle j on particle i is defined as below:

$$\mathbf{T}_i\langle\mathbf{x}_j, \mathbf{x}_i\rangle = \frac{1}{2} A \frac{\mathbf{y}_j - \mathbf{y}_i}{|\mathbf{y}_j - \mathbf{y}_i|}, \tag{3}$$

where $\mathbf{x}$ and $\mathbf{y}$ denote the positions of particles before and after deformation, respectively. The direction of the force density is along the deformed bond between the particles given by $\frac{\mathbf{y}_j-\mathbf{y}_i}{|\mathbf{y}_j-\mathbf{y}_i|}$. A is a scalar that represents the force magnitude, and it is composed of two terms by addition $A = A_{\mathrm{dil}} + A_{\mathrm{dev}}$, namely, the dilatation term A_{dil} and the deviatoric term A_{dev}.

The dilatation term A_{dil} is due to the dilatation part of deformation, i.e. volume change without any shape distortion. It is defined as

$$A_{\mathrm{dil}} = 4\omega_{ij} a \frac{\mathbf{y}_j - \mathbf{y}_i}{|\mathbf{y}_j - \mathbf{y}_i|} \cdot \frac{\mathbf{x}_j - \mathbf{x}_i}{|\mathbf{x}_j - \mathbf{x}_i|}\theta_i, \tag{4}$$

where a is a peridynamics material parameter and ω_{ij} is the weight function between particle i and particle j. For isotropic materials, ω_{ij} is monotonically decreasing with respect to the distance between particles

$$\omega_{ij} = \frac{\delta}{|\mathbf{x}_j - \mathbf{x}_i|}. \tag{5}$$

Note that ω_{ij} is defined in the material space, therefore can be pre-computed. The term θ_i measures the dilatation at particle i, which is defined with respect to the stretch of all bonds between particle i and its family:

$$\theta_i = \frac{9}{4\pi\delta^4}\sum_{k=1}^{N}\omega_{ik}s_{ik}\frac{\mathbf{y}_k - \mathbf{y}_i}{|\mathbf{y}_k - \mathbf{y}_i|}\cdot(\mathbf{x}_k - \mathbf{x}_i)V_k, \tag{6}$$

where N represents the number of family points k for point i, and V_k are their volumes. The stretch s_{ik} of the bond between particles is defined as

$$s_{ik} = \frac{|\mathbf{y}_k - \mathbf{y}_i|}{|\mathbf{x}_k - \mathbf{x}_i|} - 1. \tag{7}$$

The deviatoric term A_{dev} is a result of distortion that does not cause change in volume. It is defined with respect to the deviatoric component of bond extension:

$$A_{\mathrm{dev}} = 4\omega_{ij} b \left(e_{ij} - \frac{\delta}{4}\frac{\mathbf{y}_j - \mathbf{y}_i}{|\mathbf{y}_j - \mathbf{y}_i|}\cdot\frac{\mathbf{x}_j - \mathbf{x}_i}{|\mathbf{x}_j - \mathbf{x}_i|}\theta_i \right), \tag{8}$$

where b is a material parameter. We denote $e_{ij} = |\mathbf{y}_j - \mathbf{y}_i| - |\mathbf{x}_j - \mathbf{x}_i|$ as the extension of the bond between particle i and particle j. The term in brackets of Equation (8) is the deviatoric component of bond extension e_{ij}^d:

$$e_{ij}^d = e_{ij} - \frac{\delta}{4}\frac{\mathbf{y}_j - \mathbf{y}_i}{|\mathbf{y}_j - \mathbf{y}_i|}\cdot\frac{\mathbf{x}_j - \mathbf{x}_i}{|\mathbf{x}_j - \mathbf{x}_i|}\theta_i. \tag{9}$$

Intuitively, e_{ij}^d is constructed by removing the dilatation component of bond extension from the total bond extension e_{ij}.

In summary, the behaviour of our isotropic elastic model is controlled by two material parameters a and b. The model is equivalent to the isotropic linear elasticity model in classical theory, please refer to the supplementary document for elaborated derivation. Here, we directly provide the conversion between the material parameters in this model and those from continuum mechanics:

$$a = \frac{9\kappa}{8\pi\delta^4}, \qquad b = \frac{15\mu}{2\pi\delta^5}, \tag{10}$$

where κ and μ denote the bulk modulus and the shear modulus, respectively. In Figure 3, we demonstrate an example of the hyperelastic deformations animated with our model.

4.2. Plasticity

Plasticity model for peridynamics is less studied in literature due to its complexity. To our knowledge, Silling *et al.* [SEW*07] proposed the first plasticity model that is analogous to the von Mises flow model in classical theory. Mitchell presented a new framework for peridynamics-based plasticity modelling [Mit11] based on Silling *et al.*'s model, whereas the model has not been verified by experiments thus far. We adopt Mitchell's model for practical applications, and propose novel modifications based on their work.

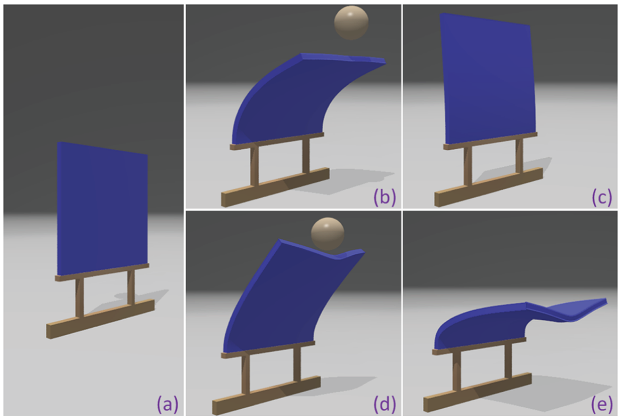

Figure 4: *Comparison of elastic and plastic deformations by shooting a sphere at two walls made of different materials with identical initial configuration as in (a). The elastic wall deforms on impact (b), and recovers afterwards (c). The plastic wall undergos permanent deformation (e) after the impact (d).*

Our plasticity model is based on purely deviatoric plastic flow theory, therefore we start by decomposing the deviatoric bond extension e^d_{ij} (see Equation (9)) into two components by addition:

$$e^d_{ij} = e^e_{ij} + e^p_{ij}, \tag{11}$$

where e^e_{ij} and e^p_{ij} are the elastic and plastic part of the total deviatoric bond extension, respectively. To incorporate plasticity into the constitutive model, the deviatoric part of internal force density (see Equation (8)) is now redefined as below:

$$A_{\text{dev}} = 4\omega_{ij} b \left(e^d_{ij} - e^p_{ij}\right) \tag{12}$$

with the contribution of plastic deviatoric bond extension removed from force computation. In case of elastic deformations, the term e^p_{ij} vanishes and Equation (12) conforms to Equation (8).

A simple yield function $f(A_{\text{dev}})$ is used to determine whether deformation has entered the plasticity regime:

$$f(A_{\text{dev}}) = \frac{(A_{\text{dev}})^2}{2} - \Psi_0, \tag{13}$$

where Ψ_0 is a critical parameter. The deformation is elastic if $f(A_{\text{dev}}) \leq 0$, and plasticity is present if $f(A_{\text{dev}}) > 0$.

In case of plastic deformations, we project A_{dev} onto the yield surface to obtain a critical value of deviatoric force density A^c_{dev}:

$$A^c_{\text{dev}} = \sqrt{2\Psi_0}\,\text{sign}(A_{\text{dev}}), \tag{14}$$

where sign$(\cdot)$ is the sign function. A^c_{dev} is used to compute the increment of plastic deviatoric bond extension:

$$\triangle e^p_n = \frac{1}{2b}(A_{\text{dev}} - A^c_{\text{dev}}), \tag{15}$$

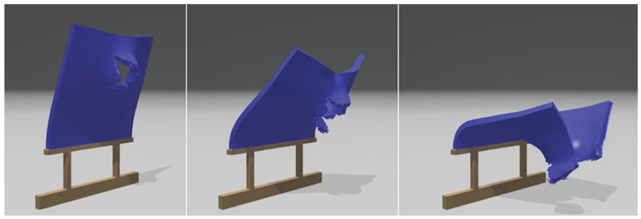

Figure 5: *Simulation of ductile fracture with different amount of maximum plasticity. From left to right, the parameter $\frac{\gamma}{|\mathbf{x}_j - \mathbf{x}_i|}$ is 0.1, 0.15 and 0.2.*

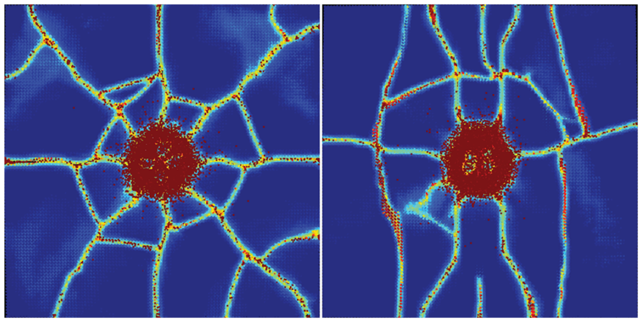

Figure 6: *Comparison of crack patterns generated by isotropic (left) and anisotropic (right) brittle fracture. The colour represents the damage of particles, with blue as no damage and red as complete damage.*

$$e^p_{n+1} = \left(e^p_n + \triangle e^p_n\right) \min\left(1, \frac{\gamma}{|e^p_n + \triangle e^p_n|}\right). \tag{16}$$

The subscripts n and $n+1$ denote the discretized point of time at which the bond extensions and corresponding increments are evaluated. The parameter γ which does not appear in the original model of Mitchell's [Mit11] is used to enforce a limit on the amount of plasticity. We found in experiments that with this parameter we obtain more control over the plastic behaviours (see Figure 5) and the stability of simulation is improved as well. Figure 4 shows a comparison of the simulation results using our elastoplastic constitutive model. Our elastic model produces correct elastic behaviours, and permanent deformation is captured when plasticity is involved.

4.3. Anisotropy

Our constitutive model is isotropic up to now, and we extend it to anisotropy in this section. We model anisotropy by manipulating the weight functions between particles (see Equation (5)) with direction information. The key idea is to associate an anisotropy matrix $\mathbf{G}$ with each particle, so that applying the transformation to the bond between particles biases the influence weight towards preferred directions. The weight function ω_{ij} for anisotropic materials is computed as below:

$$\omega_{ij} = \frac{\delta}{|\mathbf{G}(\mathbf{x}_j - \mathbf{x}_i)|}. \tag{17}$$

Appealing anisotropic effects could be generated with our anisotropy model. See Figure 1 for a demonstration of the model applied to brittle and ductile fracture animation. Figure 6 compares the crack patterns generated by the brittle fracture examples in Figure 1.

5. Fracture

In this section, we present our fracture model and introduce the mesh embedding strategy we employ to generate crack surfaces.

5.1. Fracture criterion

Material damage can be modelled in peridynamics by permanently eliminating the bonds between particles. The dynamics with discontinuities is trivial due to the integral-based nature of peridynamics. For elastic brittle materials, a simple critical stretch is generally used as the fracture criterion. This criterion conforms to the physically plausible energy release rate, and it has been validated before [SA05]. Levine *et al.* [LBC*14] also utilized this criterion for brittle fracture modelling in computer graphics. In order to account for plasticity and model ductile fracture, we redefined the elastic critical stretch criterion as

$$s_{ij}^{e} = \frac{e_{ij} - e_{ij}^{p}}{|\mathbf{x}_i - \mathbf{x}_j|}. \tag{18}$$

Unfortunately, we found in experiments that this fracture criterion would cause unrealistic artefacts since bonds with smaller rest lengths are sometimes more prone to breaking. We alleviate this problem by incorporating the weight function ω_{ij} into the criterion to increase the fracture criterion of closer family members. Shattering effects could arise for brittle materials, which lead to many tiny fragments. We could avoid the generation of too small fragments by continuously increasing the crack threshold as the material gets damaged. The final fracture criterion that we employ in our model is formulated as below:

$$s_{ij}^{\omega} = (1 + \alpha\phi)\frac{s_{ij}^{e}}{\omega_{ij}} = (1 + \alpha\phi)\frac{e_{ij} - e_{ij}^{p}}{\delta}, \tag{19}$$

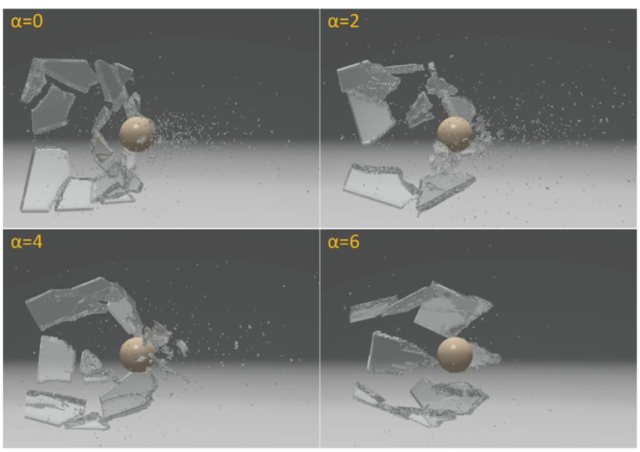

Figure 7: *Glass wall fracture with different α values.*

where $\phi = 1 - \frac{n_i}{N_i}$ measures the damage level of material point i. n_i and N_i are the numbers of active bonds connecting i with its family members in the deformed and initial configurations, respectively. n_i gradually decreases as more bonds around i are broken, increasing the damage level of i. The parameter α is set to 0 by default, and could be used to mitigate the shattering effect while non-zero values are given. Figure 7 provides an example of controlling the dust with different α values. It shows that our criterion is able to produce compelling results in practical use.

5.2. Embedded mesh

While particle-based discretization offers great simplicity, this simplicity does come at a cost that it is difficult to generate surface representation. This naturally motivates the use of mesh embedding approach, in which the boundary of volumetric meshes could represent the original object surface and the newly generated crack surfaces during simulation. We use tetrahedron meshes to represent object geometry, and the particles are initialized at the barycentres of each mesh element. The particle family members are initialized according to the mesh connectivity and a pre-specified horizon δ. To accommodate the topology changes resulted from fracture, we propose a simple strategy that dynamically split the embedded mesh along the elements.

We achieve this by maintaining a crack face set and continuously adding the shared triangles to it for fracture happened between immediate elements. At each time step, we investigate merely those vertices that involved in crack face set and determine whether its connected tetrahedra have been separated by crack faces. If this is the case, we split the vertex, assign corresponding tetrahedra to each of them, and make a topological change on the embedded mesh. After splitting, we could safely remove only those crack faces that directly results in our vertex splitting. If the connected tetrahedra are separated into more than two groups, we accordingly split vertex into multiple copies. Simultaneous splitting of multiple vertices at one crack face are also compatible in our method. Figure 8 shows an example of using our strategy to produce complex crack surfaces.

After handling mesh topology, we update the vertex positions using the velocities of corresponding particles. A simple weighted-average approach is employed to update the vertex positions:

$$\omega_{\mathrm{v}} = \sum_{\mathrm{p}} \frac{1}{4} m_{\mathrm{p}}, \tag{20}$$

$$\mathbf{v}_{\mathrm{v}} = \frac{1}{\omega_{\mathrm{v}}} \sum_{\mathrm{p}} \frac{1}{4} m_{\mathrm{p}} \mathbf{v}_{\mathrm{p}}, \tag{21}$$

$$\mathbf{x}_{\mathrm{v}}^{t+1} = \mathbf{x}_{\mathrm{v}}^{t} + \Delta t \mathbf{v}_{\mathrm{v}}, \tag{22}$$

where subscripts p and v represent the particle and the mesh vertex, respectively. m_{p} and $\mathbf{v}_{\mathrm{p}}$ are the mass and velocity of the particle, $\mathbf{v}_{\mathrm{v}}$ and $\mathbf{x}_{\mathrm{v}}$ are the velocity and position of the mesh vertex.

6. Results

We present the results produced with our method in this section. All our examples are run on a 3.5 GHz, Intel Core i7-5930K CPU with 32 G RAM. The embedded tetrahedron meshes are generated

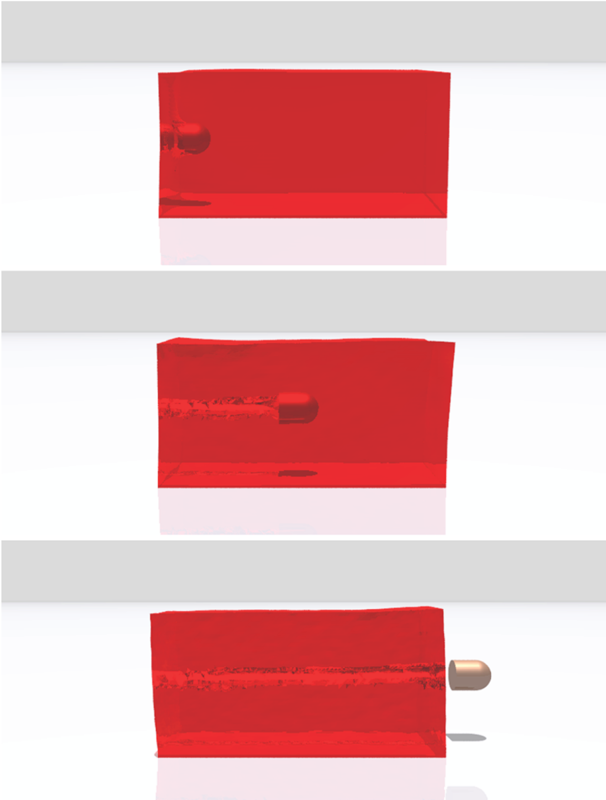

Figure 8: *Shooting a bullet through a jello, producing complex crack surfaces.*

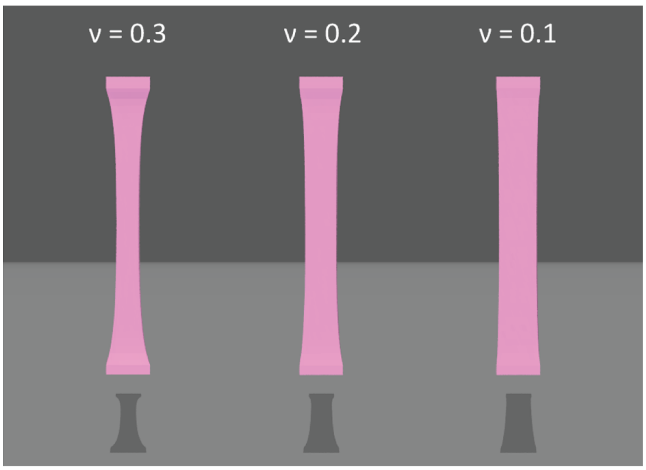

Figure 9: *Simulation of stretching beams with different Poisson ratios.*

using the open-source TetGen software [Si15]. All the figures in the paper are rendered offline using the open-source POV-Ray software (http://www.povray.org/). We use explicit time integration for ease of implementation. We also performed a naive parallelized implementation of our method using OpenMP.

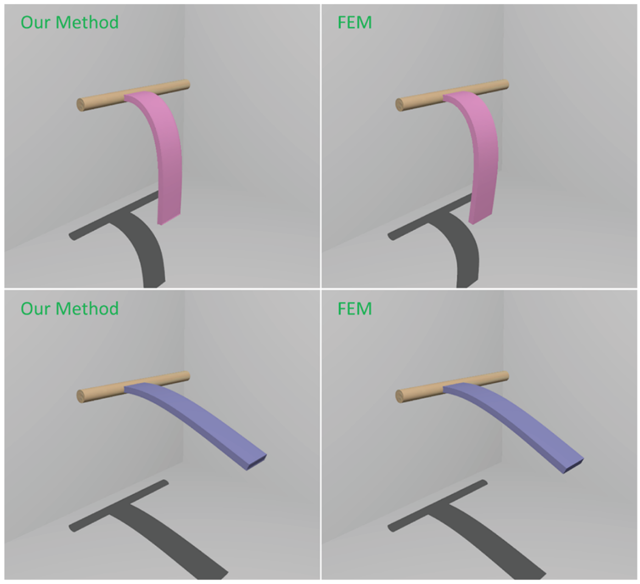

Figure 10: *Simulation of bending beams with different stiffness (top: soft; bottom: stiff) using our method and FEM. The results of our method are indistinguishable from the results produced by FEM.*

Constitutive model validation. We validate our constitutive model by simulating deformations with varied material properties and performing comparisons with the results of FEM. Figure 3 shows an example of isotropic elastic deformations, where the back and four limbs of an armadillo are initially anchored and then the anchor on the back is removed. The deformations are plausible and no undesirable numerical fracture occurs when the arms of the armadillo are overstretched. In Figure 4, we compare the results of elasticity and plasticity, and our model produces correct deformation behaviours. Figure 5 demonstrates the varied effects produced by tuning the amount of maximum plasticity. Figure 9 compares the elastic deformations of stretching beams with different Poisson ratio values. Unlike Levine *et al.*'s model [LBC*14], our constitutive model is not limited to a single Poisson ratio. Finally, we conduct comparisons with FEM through Figures 10–13. The deformations of a bending beam in Figure 10 produced with our method are almost identical to those generated by FEM, under both stiff and soft material settings. We further demonstrate the accuracy of our method in constitutive modelling using comparisons with quantitative error analysis. The swing (see Figure 11) and twist (see Figure 12) deformations of the bar produced by our method are as accurate as those by corotated linear FEM with position deviations less than 10%. The position deviations are measured over the diagonal of the object's bounding box: $Error = \frac{|x_p - x_p^{ref}|}{d}$ where d is the length of the diagonal. Note that our constitutive model alleviates artefacts of the classical linear model albeit derived from it. It is because peridynamics does not employ the geometric linear approximation as the Cauchy strain in continuum mechanics does. Thus peridynamics does not suffer from ghost forces while undergoing rigid rotations. We also obtain nice accuracy for the non-cyclic vibrations of the armadillo presented in Figure 13. Therefore, we

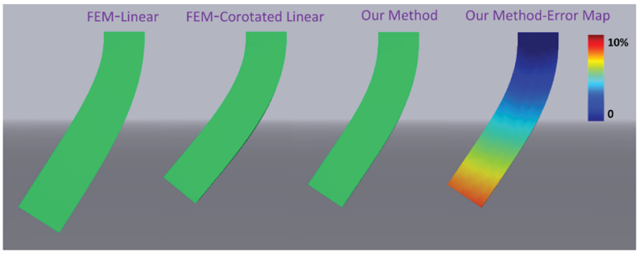

Figure 11: *Simulation of a swinging bar using linear FEM (left), corotated linear FEM (middle left) and our method (middle right). Our method is accurate as the corotated linear FEM (right).*

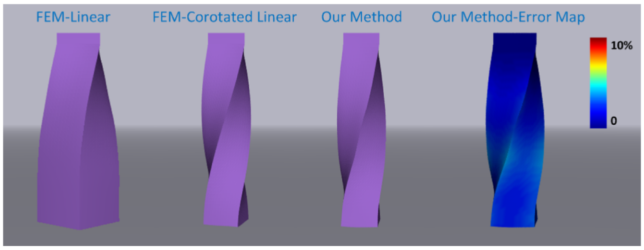

Figure 12: *Simulation of a twisting bar using linear FEM (left), corotated linear FEM (middle left) and our method (middle right). Our method is accurate as the corotated linear FEM (right).*

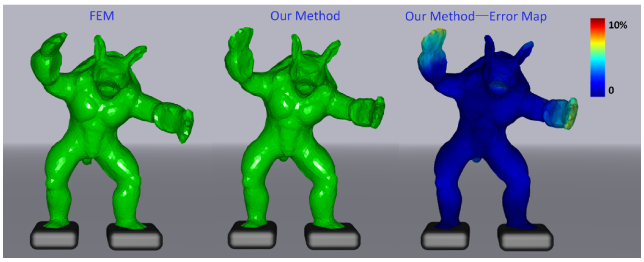

Figure 13: *Simulation of noncyclic vibrations for an armadillo using FEM (left) and our method (middle). The accuracy of our method is acceptable compared with FEM (right).*

believe our peridynamics-based constitutive model is plausible for graphical animations.

Fracture animation. Our method could simulate brittle and ductile fracture with compelling visual realism. In Figure 1, a wide range of fracture behaviours are generated, including isotropic brittle fracture, anisotropic brittle fracture, isotropic ductile fracture and anisotropic ductile fracture. This demonstrates the capability of our method in simulating fracture. We believe our approach is the first peridynamics-based framework in graphics with such flexibility. Figure 8 shows an example of shooting a bullet into a jello-like object. Our method handles well the generation of the complex crack surfaces. The armadillo in Figure 14 is stretched until its limbs tear off. The behaviour of ductile fracture is correctly demonstrated, including the progressive generation of multiple cracks (see Figure 18). The glass wall in Figure 15 is pressed by a heavy metal ball. Cracks develop and propagate without shattering the glass into fragments. This phenomenon cannot be reproduced by the level set approach [HJST13] as mentioned in their paper, and it is challenging for the remeshing-based FEM methods [OH99, OBH02] considering the mesh operations. In contrast, our method handles the complicated propagation process well, including the branching and merging of cracks. The approach by Pauly *et al.* [PKA*05] could produce results comparable to ours, employing explicit handling of the topology events. Our method, however, requires none. In Figure 16, a bunny made of elastic material falls to the ground and shatters. Our method is able to realistically capture the secondary fracture of the fragments. Figure 17 is another demonstration of our method in handling crack tips. A thin sheet with initial cracks is torn on two sides. The cracks gradually proceed and finally shatter the sheet. Please note the filaments generated as a result of crack branching and merging.

Choice of δ. We use a δ value of 1.0λ for most of the FEM comparisons, where λ is the average edge length of the embedded tetrahedron mesh. As peridynamics converges to classical continuum mechanics while δ approaches zero [WA05], this specific choice of δ amounts to the nodal force computation of FEM using the 1-ring neighbours. Although not always necessary, fine-tuning the δ value is a viable way of getting well-synchronized results. For instance, in Figure 13, we adjust it to 1.38λ to achieve our best result. We studied the effect of different δ values with experiments, and the results reveal that simulation plausibility is not very sensitive to

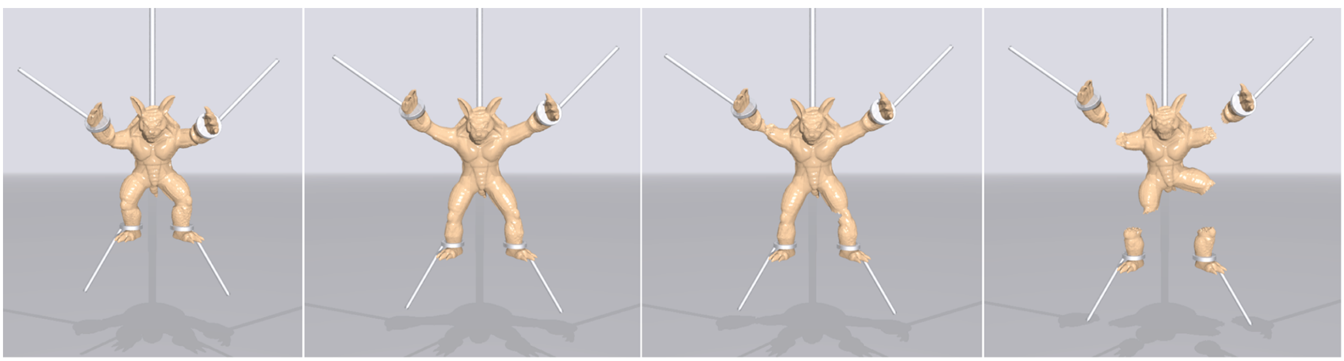

Figure 14: *An armadillo is stretched until its limbs tear off.*

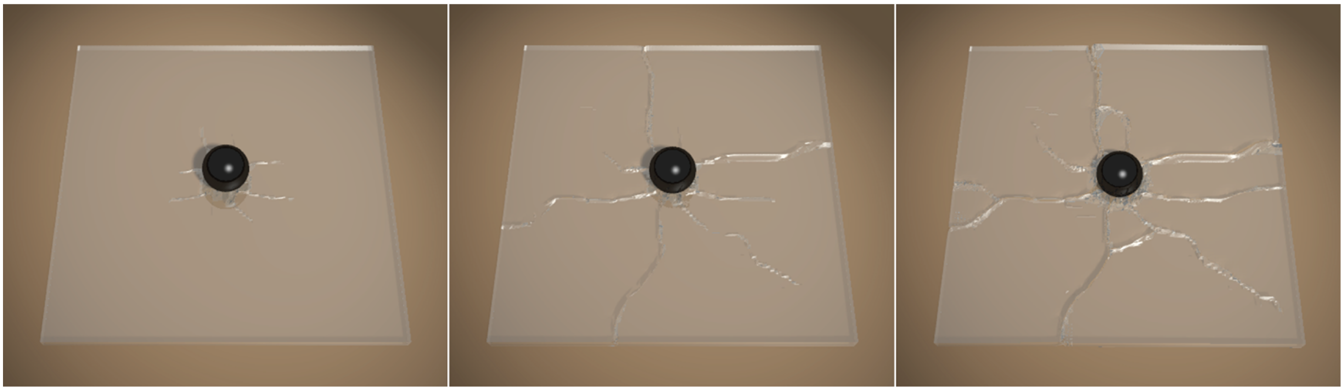

Figure 15: *A glass wall on ground is pressed by a heavy metal ball and cracks without separating. Our method can model the complicated crack propagation process, including branching and merging.*

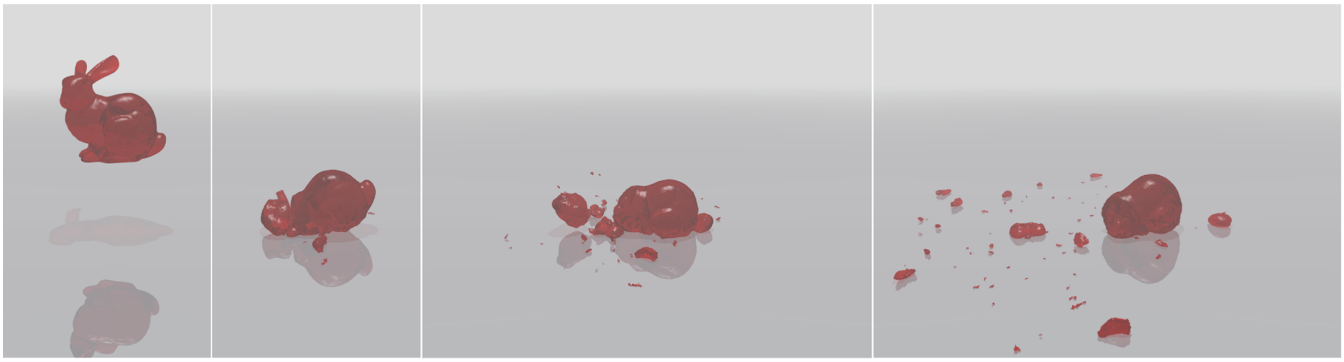

Figure 16: *An elastic bunny falls to the ground and shatters into pieces. Note the secondary fracture of the fragments.*

the parameter δ. In practice, we recommend a value in the range between 1.0λ and 2.0λ. Larger values could result in inadequate family members for particles close to object boundary, causing the material to behave softer than it should be. In this case, a correction for boundary particles needs to be taken into account. Please refer to the accompanied video for the comparison of different δ values.

In Table 1, we list the detailed parameter settings and the performance data for all the examples presented in the paper. The results in this paper are produced with practical computation time. Note that we employ damping forces in a few of the examples, mainly to ease the burden of self-collision handling, which is not the major concern of this work. The experimented damping models include a simple air damping $\mathbf{v}_{\text{new}} = (1 - \lambda_a)\mathbf{v}_{\text{old}}$, and a Laplacian smoothing $\mathbf{v}_{\text{new}} = \mathbf{v}_{\text{old}} + \lambda_l \mathbf{L}(\mathbf{v}_{\text{old}})$. Please refer to Table 1 for the specific values of the damping coefficients λ_a and λ_l in each example. Although effective in practice, these damping forces are not a necessity for our method since the issue of self-penetration could be (and should be) addressed by superior detection and resolution strategies.

7. Discussions

We have introduced a novel meshless framework for graphical modelling and animation of elastoplastic solids. Our work is the first peridynamics-based framework in computer graphics that can simulate a wide range of material behaviours, including elasticity, plasticity and fracture.

Our work is not without limitations. Currently, we cannot afford large time steps because we used explicit time integration in our implementation. In the future, we plan to incorporate implicit time integration into our framework to achieve less restricted time step size. Another limitation of our work stems from the mesh embedding strategy for crack surface representation. The level of crack detail is highly dependent on the embedded mesh resolution. In addition, we generate crack surfaces by separating the mesh elements, which could cause the zig-zag artefact (see Figure 18). This artefact might be alleviated by smoothing the crack surfaces somewhat, or employing the virtual node algorithm. While we used multi-threading in our implementation, the performance of our method could be further improved with general purpose graphics processing units (GPGPU) techniques.

Other interesting avenues for future work include combining peridynamics theory with existing methods from classical theory such as FEM and SPH. These methods complement each other, and their combination could produce a new method that is more powerful for animation production.

Table 1: *Model information, simulation parameters and performance data for all our examples. λ is the average edge length of the embedded tetrahedron mesh used for particle initiation.*

Examples	Particle num	δ	Bond num	κ (KPa)	μ (KPa)	ρ (Kg/m^3)	Ψ_0	$\frac{\gamma}{\lvert\mathbf{x}_j-\mathbf{x}_i\rvert}$	$s^w_{(k)(j)}$	Δt (s)	λ_a	λ_l	Performance (s/step)
Glass Wall [Figure 1(a)(b), 7, 15]	3.0×10^5	1.45λ	5.0×10^7	3.3×10^7	2.0×10^7	2200	∞	0.0	0.0005	1.0×10^{-6}	0	0	~ 2.4
Plastic Wall [Figure 1(c)(d)]	3.0×10^5	1.45λ	5.0×10^7	3.3×10^3	2.0×10^3	2200	10^{25}	0.2	0.05	1.0×10^{-4}	0.002	0	~ 2.4
Armadillo [Figure 3]	4.2×10^5	1.50λ	7.5×10^7	6.3×10^4	3.8×10^4	1000	∞	0.0	∞	1.0×10^{-4}	0.002	0.001	~ 5.3
Elastic Wall [Figure 4(a)(d)]	3.0×10^5	1.45λ	5.0×10^7	1.0×10^4	6.0×10^3	1200	∞	0.0	∞	5.0×10^{-5}	0	0	~ 2.4
Plastic Wall [Figure 4(d)(e)]	3.0×10^5	1.45λ	5.0×10^7	1.0×10^4	6.0×10^3	1200	10^{26}	0.2	∞	5.0×10^{-5}	0.0005	0	~ 2.4
Wall [Figure 5]	3.0×10^5	1.45λ	5.0×10^7	1.0×10^4	6.0×10^3	1200	10^{26}	(0.1, 0.15, 0.2)	∞	5.0×10^{-5}	0.0005	0	~ 2.4
Jello [Figure 8]	4.6×10^5	1.45λ	8.6×10^7	1.0×10^3	4.6×10^2	1000	∞	0.0	0.4	5.0×10^{-5}	0	0	~ 3.8
Beam Stretch [Figure 9]	2.2×10^4	$1.0\,\lambda$	1.3×10^6	2.0×10^3	$(9.2, 1.5, 2.2) \times 10^2$	1000	∞	0.0	∞	1.0×10^{-5}	0	0	~ 0.2
Soft Beam Bend [Figure 10]	4.5×10^4	$1.0\,\lambda$	6.9×10^6	6.3×10^3	3.8×10^3	1000	∞	0.0	∞	5.0×10^{-5}	0	0	~ 0.6
Stiff Beam Bend [Figure 10]	4.5×10^4	$1.0\,\lambda$	6.9×10^6	3.3×10^4	2.0×10^4	1000	∞	0.0	∞	2.5×10^{-5}	0	0	~ 0.6
Bar Swing [Figure 11]	9.2×10^3	$1.11\,\lambda$	1.5×10^5	5.0×10^3	5.0×10^3	1000	∞	0.0	∞	1.0×10^{-4}	0	0	~ 0.05
Bar Twist [Figure 12]	9.2×10^3	$1.34\,\lambda$	1.5×10^5	1.0×10^3	6.0×10^2	1000	∞	0.0	∞	1.0×10^{-4}	0	0	~ 0.06
Armadillo Vibrate [Figure 13]	2.0×10^4	$1.38\,\lambda$	1.8×10^6	5.0×10^3	3.0×10^3	1000	∞	0.0	∞	5.0×10^{-4}	0	0	~ 0.2
Armadillo [Figure 14]	4.2×10^5	1.50λ	7.5×10^7	6.3×10^4	3.8×10^4	1000	∞	0.0	0.61	1.0×10^{-4}	0	0.001	~ 5.3
Bunny [Figure 16]	5.2×10^5	1.45λ	8.8×10^7	2.5×10^2	1.2×10^2	1000	∞	0.0	0.13	5.0×10^{-4}	0	0	~ 5.2
Thin Sheet [Figure 17]	1.6×10^5	1.45λ	2.0×10^7	5.0×10^3	3.0×10^3	1000	∞	0.0	0.1	5.0×10^{-5}	0	0.001	~ 1.8

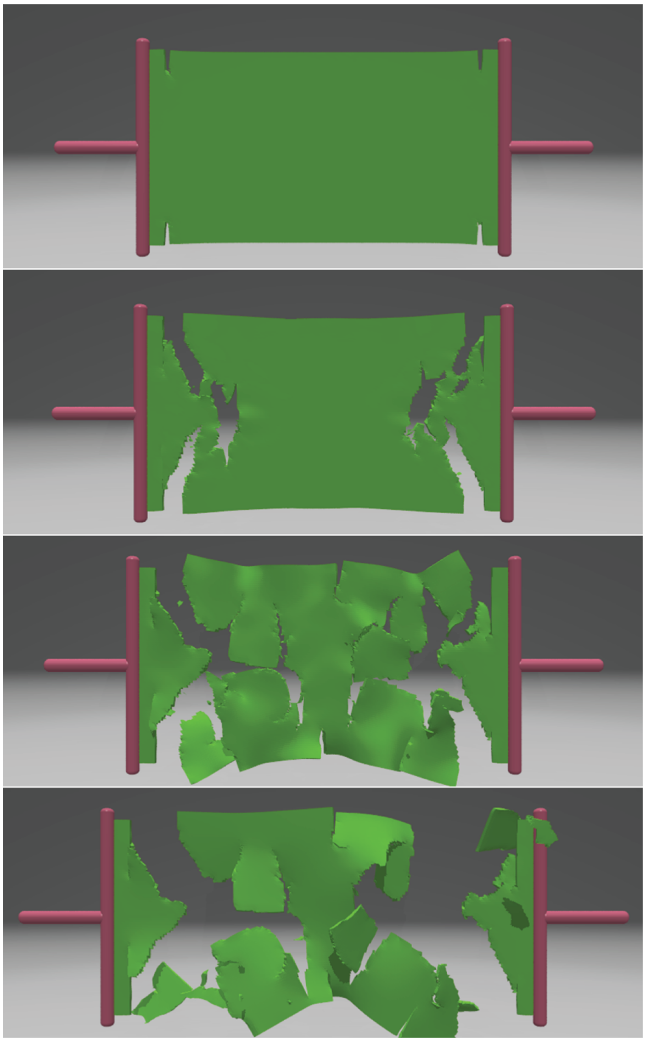

Figure 17: *A thin sheet with initial cracks is torn apart. The cracks proceed with branching and merging, separating the sheet into pieces.*

Acknowledgements

We acknowledge the anonymous reviewers for their comments and suggestions that greatly improve our work. The authors would also like to thank Xiaowei He, Sheng Yang and Liyou Xu for discussions during our research. The work is supported by Grant No. 2015BAK01B06 from The National Key Technology Research and Development Program of China, and Grant No. 61232014, 61421062, 61170205, 61472010 from National Natural Science Foundation of China.

References

[ABL*08] Askari E., Bobaru F., Lehoucq R., Parks M., Silling S., Weckner O.: Peridynamics for multiscale materials modeling. *Journal of Physics: Conference Series 125* (2008), 12–78.

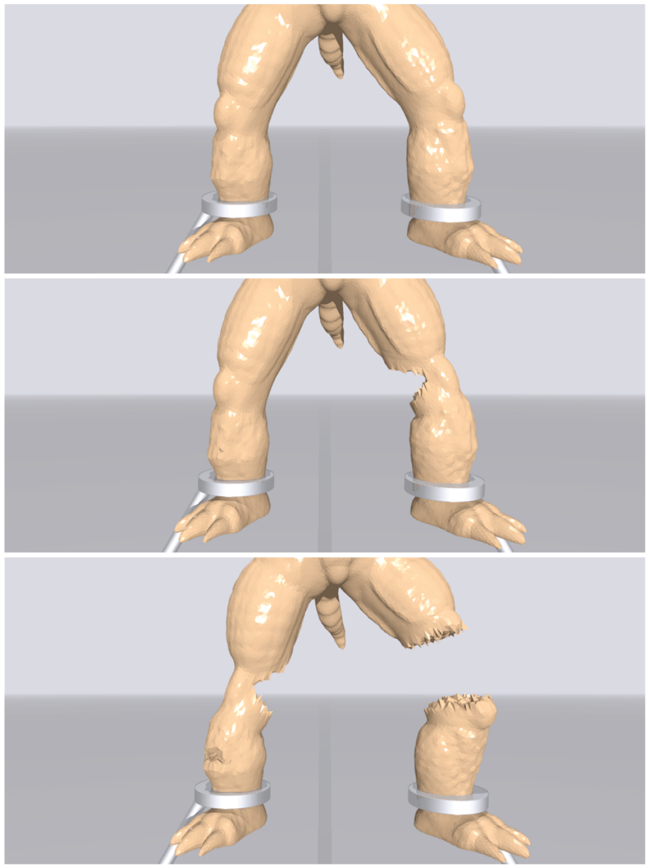

Figure 18: *A close view of the progressive fracture of the armadillo's legs.*

[AXS06] Askari E., Xu J., Silling S.: Peridynamic analysis of damage and failure in composites. In *Proceedings of the 44th AIAA Aerospace Sciences Meeting and Exhibit* (Reno, Nevada, 2006), Reston, VA: AIAA.

[BG00] Bielser D., Gross M. H.: Interactive simulation of surgical cuts. In *PG '00: Proceedings of the 8th Pacific Conference on Computer Graphics and Applications* (Washington, DC, USA, 2000), IEEE Computer Society, pp. 116–125.

[BHTF07] Bao Z., Hong J.-M., Teran J., Fedkiw R.: Fracturing rigid materials. *IEEE Transactions on Visualization and Computer Graphics 13*, 2 (Mar. 2007), 370–378.

[BWHT07] Bargteil A. W., Wojtan C., Hodgins J. K., Turk G.: A finite element method for animating large viscoplastic flow. *ACM Transactions on Graphics 26*, 3 (July 2007), 16:1–16:8.

[ELP13] Emmrich E., Lehoucq R. B., Puhst D.: Peridynamics: A nonlocal continuum theory. In *Meshfree Methods for Partial Differential Equations VI*. Springer, Berlin, Germany (2013), pp. 45–65.

[FDA02] Forest C., Delingette H., Ayache N.: Removing tetrahedra from a manifold mesh. In *Proceedings of Computer*

Animation (Geneva, Switzerland, Switzerland, 2002), IEEE, pp. 225–229.

[GBB09] GERSZEWSKI D., BHATTACHARYA H., BARGTEIL A. W.: A point-based method for animating elastoplastic solids. In *SCA '09: Proceedings of the 2009 ACM SIGGRAPH/Eurographics Symposium on Computer Animation* (New York, NY, USA, 2009), ACM, pp. 133–138.

[GMD13] GLONDU L., MARCHAL M., DUMONT G.: Real-time simulation of brittle fracture using modal analysis. *IEEE Transactions on Visualization and Computer Graphics 19*, 2 (2013), 201–209.

[HJST13] HEGEMANN J., JIANG C., SCHROEDER C., TERAN J. M.: A level set method for ductile fracture. In *SCA '13: Proceedings of the 12th ACM SIGGRAPH/Eurographics Symposium on Computer Animation* (New York, NY, USA, 2013), ACM, pp. 193–201.

[HW15] HAHN D., WOJTAN C.: High-resolution brittle fracture simulation with boundary elements. *ACM Transactions on Graphics 34*, 4 (July 2015), 151:1–151:12.

[ITF04] IRVING G., TERAN J., FEDKIW R.: Invertible finite elements for robust simulation of large deformation. In *SCA '04: Proceedings of the 2004 ACM SIGGRAPH/Eurographics Symposium on Computer Animation* (Aire-la-Ville, Switzerland, 2004), Eurographics Association, pp. 131–140.

[KMB*09] KAUFMANN P., MARTIN S., BOTSCH M., GRINSPUN E., GROSS M.: Enrichment textures for detailed cutting of shells. *ACM Transactions on Graphics 28*, 3 (July 2009), 50:1–50:10.

[LBC*14] LEVINE J. A., BARGTEIL A. W., CORSI C., TESSENDORF J., GEIST R.: A peridynamic perspective on spring-mass fracture. In *SCA '14: Proceedings of the ACM SIGGRAPH/Eurographics Symposium on Computer Animation* (Aire-la-Ville, Switzerland, 2014), Eurographics Association, pp. 47–55.

[LHLW11] LIU N., HE X., LI S., WANG G.: Meshless simulation of brittle fracture. *Computer Animation & Virtual Worlds 22*, 2–3 (Apr. 2011), 115–124.

[LZLW11] LIU N., ZHU F., LI S., WANG G.: Anisotropic kernels for meshless elastic solids. In *CADGRAPHICS '11: Proceedings of the 12th International Conference on Computer-Aided Design and Computer Graphics* (Washington, DC, USA, 2011), IEEE Computer Society, pp. 349–356.

[MBF04] MOLINO N., BAO Z., FEDKIW R.: A virtual node algorithm for changing mesh topology during simulation. *ACM Transactions on Graphics 23*, 3 (Aug. 2004), 385–392.

[MBP14] MUGUERCIA L., BOSCH C., PATOW G.: Fracture modeling in computer graphics. *Computers & Graphics 45* (2014), 86–100.

[MCG03] MÜLLER M., CHARYPAR D., GROSS M.: Particle-based fluid simulation for interactive applications. In *SCA '03: Proceedings of the 2003 ACM SIGGRAPH/Eurographics Symposium on Computer Animation* (Aire-la-Ville, Switzerland, 2003), Eurographics Association, pp. 154–159.

[MCK13] MÜLLER M., CHENTANEZ N., KIM T.-Y.: Real time dynamic fracture with volumetric approximate convex decompositions. *ACM Transactions on Graphics 32*, 4 (July 2013), 115:1–115:10.

[MG04] MÜLLER M., GROSS M.: Interactive virtual materials. In *GI '04: Proceedings of Graphics Interface 2004* (School of Computer Science, University of Waterloo, Waterloo, Ontario, Canada, 2004), Canadian Human-Computer Communications Society, pp. 239–246.

[Mit11] MITCHELL J. A.: *A nonlocal, ordinary, state-based plasticity model for peridynamics*. SAND report 7597, 2011.

[MK00] MOR A. B., KANADE T.: Modifying soft tissue models: Progressive cutting with minimal new element creation. In *MICCAI '00: Proceedings of the Third International Conference on Medical Image Computing and Computer-Assisted Intervention* (London, UK, 2000), Springer-Verlag, pp. 598–607.

[MKN*04] MÜLLER M., KEISER R., NEALEN A., PAULY M., GROSS M., ALEXA M.: Point based animation of elastic, plastic and melting objects. In *SCA '04: Proceedings of the 2004 ACM SIGGRAPH/Eurographics Symposium on Computer Animation* (Aire-la-Ville, Switzerland, 2004), Eurographics Association, pp. 141–151.

[MMA99] MAZARAK O., MARTINS C., AMANATIDES J.: Animating exploding objects. In *Proceedings of the 1999 Conference on Graphics Interface '99* (San Francisco, CA, USA, 1999), Morgan Kaufmann Publishers Inc., pp. 211–218.

[MMDJ01] MÜLLER M., MCMILLAN L., DORSEY J., JAGNOW R.: Real-time simulation of deformation and fracture of stiff materials. In *Proceedings of the Eurographic Workshop on Computer Animation and Simulation* (New York, NY, USA, 2001), Springer-Verlag New York, Inc., pp. 113–124.

[MO14] MADENCI E., OTERKUS E.: *Peridynamic Theory and Its Applications*. Springer, Berlin, Germany, 2014.

[NF99] NEFF M., FIUME E.: A visual model for blast waves and fracture. In *Proceedings of the 1999 Conference on Graphics Interface '99* (San Francisco, CA, USA, 1999), Morgan Kaufmann Publishers Inc., pp. 193–202.

[NTB*91] NORTON A., TURK G., BACON B., GERTH J., SWEENEY P.: Animation of fracture by physical modeling. *Visual Computer 7*, 4 (July 1991), 210–219.

[OBH02] O'BRIEN J. F., BARGTEIL A. W., HODGINS J. K.: Graphical modeling and animation of ductile fracture. *ACM Transactions on Graphics 21*, 3 (July 2002), 291–294.

[OH99] O'BRIEN J. F., HODGINS J. K.: Graphical modeling and animation of brittle fracture. In *SIGGRAPH '99: Proceedings of the 26th Annual Conference on Computer Graphics and Interactive Techniques* (New York, NY, USA, 1999), ACM Press/Addison-Wesley Publishing Co., pp. 137–146.

[PKA*05] PAULY M., KEISER R., ADAMS B., DUTRÉ P., GROSS M., GUIBAS L. J.: Meshless animation of fracturing solids. *ACM Transactions on Graphics 24*, 3 (July 2005), 957–964.

[PO09] PARKER E. G., O'BRIEN J. F.: Real-time deformation and fracture in a game environment. In *SCA '09: Proceedings of the 2009 ACM SIGGRAPH/Eurographics Symposium on Computer Animation* (New York, NY, USA, 2009), ACM, pp. 165–175.

[SA05] SILLING S. A., ASKARI E.: A meshfree method based on the peridynamic model of solid mechanics. *Computers and Structures 83*, 17–18 (June 2005), 1526–1535.

[SA14] SILLING S. A., ASKARI A.: *Peridynamic model for fatigue cracking*. Technical Report, Sandia National Laboratories (SNL-NM), Albuquerque, NM (United States), 2014.

[SB12] SIFAKIS E., BARBIC J.: FEM simulation of 3D deformable solids: A practitioner's guide to theory, discretization and model reduction. In *ACM SIGGRAPH 2012 Courses* (New York, NY, USA, 2012), SIGGRAPH '12, ACM, pp. 20:1–20:50.

[SC14] SILLING S. A., COX J. V.: *Hierarchical multiscale method development for peridynamics*. SAND Report 18565, 2014.

[SDF07] SIFAKIS E., DER K. G., FEDKIW R.: Arbitrary cutting of deformable tetrahedralized objects. In *SCA '07: Proceedings of the 2007 ACM SIGGRAPH/Eurographics Symposium on Computer Animation* (Aire-la-Ville, Switzerland, 2007), Eurographics Association, pp. 73–80.

[SEW*07] SILLING S. A., EPTON M., WECKNER O., XU J., ASKARI E.: Peridynamic states and constitutive modeling. *Journal of Elasticity 88*, 2 (2007), 151–184.

[Si15] SI H.: TetGen, a Delaunay-based quality tetrahedral mesh generator. *ACM Transactions on Mathematical Software 41*, 2 (Feb. 2015), 11:1–11:36.

[Sil00] SILLING S.: Reformulation of elasticity theory for discontinuities and long-range forces. *Journal of the Mechanics and Physics of Solids 48*, 1 (2000), 175–209.

[SO14] SCHVARTZMAN S. C., OTADUY M. A.: Fracture animation based on high-dimensional Voronoi diagrams. In *I3D '14: Proceedings of the 18th Meeting of the ACM SIGGRAPH Symposium on Interactive 3D Graphics and Games* (New York, NY, USA, 2014), ACM, pp. 15–22.

[SOG09] STEINEMANN D., OTADUY M. A., GROSS M.: Splitting meshless deforming objects with explicit surface tracking. *Graphical Models 71*, 6 (Nov. 2009), 209–220.

[SSC*13] STOMAKHIN A., SCHROEDER C., CHAI L., TERAN J., SELLE A.: A material point method for snow simulation. *ACM Transactions on Graphics 32*, 4 (July 2013), 102:1–102:10.

[SWAB10] SILLING S., WECKNER O., ASKARI E., BOBARU F.: Crack nucleation in a peridynamic solid. *International Journal of Fracture 162*, 1–2 (2010), 219–227.

[SWB01] SMITH J., WITKIN A., BARAFF D.: Fast and controllable simulation of the shattering of brittle objects. *Computer Graphics Forum 20*, 2 (2001), 81–90.

[TF88] TERZOPOULOS D., FLEISCHER K.: Modeling inelastic deformation: Viscolelasticity, plasticity, fracture. *ACM SIGGRAPH Computer Graphics 22*, 4 (June 1988), 269–278.

[TPBF87] TERZOPOULOS D., PLATT J., BARR A., FLEISCHER K.: Elastically deformable models. *ACM SIGGRAPH Computer Graphics 21*, 4 (Aug. 1987), 205–214.

[TSIF05] TERAN J., SIFAKIS E., IRVING G., FEDKIW R.: Robust quasistatic finite elements and flesh simulation. In *SCA '05: Proceedings of the 2005 ACM SIGGRAPH/Eurographics Symposium on Computer Animation* (New York, NY, USA, 2005), ACM, pp. 181–190.

[WA05] WECKNER O., ABEYARATNE R.: The effect of long-range forces on the dynamics of a bar. *Journal of the Mechanics and Physics of Solids 53*, 3 (2005), 705–728.

[WJST14] WANG Y., JIANG C., SCHROEDER C., TERAN J.: An adaptive virtual node algorithm with robust mesh cutting. In *SCA '14: Proceedings of the ACM SIGGRAPH/Eurographics Symposium on Computer Animation* (Aire-la-Ville, Switzerland, 2014), Eurographics Association, pp. 77–85.

[WWD15] WU J., WESTERMANN R., DICK C.: A survey of physically based simulation of cuts in deformable bodies. *Computer Graphics Forum 34*, 6 (Sept. 2015), 161–187.

[ZBG15] ZHU Y., BRIDSON R., GREIF C.: Simulating rigid body fracture with surface meshes. *ACM Transactions on Graphics 34*, 4 (July 2015), 150:1–150:11.

[ZZL*16] ZHU F., ZHAO J., LI S., TANG Y., WANG G.: Dynamically enriched MPM for invertible elasticity. *Computer Graphics Forum* (2016).

Supporting Information

Additional Supporting Information may be found in the online version of this article at the publisher's web site:

Supplementary Technical Document: It presents the derivation of the constitutive model.

Video S1